

Morphology of urethral tissues

Bert Müller*^a, Georg Schulz^a, Julia Herzen^b, Shpend Mushkolaj^a, Therese Bormann^a,
Felix Beckmann^b, Klaus Püschel^c

^aBiomaterials Science Center, University of Basel, 4031 Basel, Switzerland;

^bInstitute for Materials Research, GKSS-Research Centre, 21502 Geesthacht, Germany;

^cInstitute for Legal Medicine, University Hospital Hamburg-Eppendorf, 22529 Hamburg, Germany

ABSTRACT

Micro computed tomography has been developed to a powerful technique for the characterization of hard and soft human and animal tissues. Soft tissues including the urethra, however, are difficult to be analyzed, since the microstructures of interest exhibit X-ray absorption values very similar to the surroundings. Selective staining using highly absorbing species is a widely used approach, but associated with significant tissue modification. Alternatively, one can suitably embed the soft tissue, which requires the exchange of water. Therefore, the more recently developed phase contrast modes providing much better contrast of low X-ray absorbing species are especially accommodating in soft tissue characterization. The present communication deals with the morphological characterization of sheep, pig and human urethras on the micrometer scale taking advantage of micro computed tomography in absorption and phase contrast modes. The performance of grating-based tomography is demonstrated for freshly explanted male and female urethras in saline solution. The micro-morphology of the urethra is important to understand how the muscles close the urethra to reach continence. As the number of incontinent patients is steadily increasing, the function under static and, more important, under stress conditions has to be uncovered for the realization of artificial urinary sphincters, which needs sophisticated, biologically inspired concepts to become nature analogue.

Keywords: urethra, micro computed tomography, grating interferometry, urinary incontinence

1. INTRODUCTION

Urethral tissue exhibits characteristic properties, not present in man-made engineering products. Therefore, it is impossible to find a tube that has the liquid-like properties [1] and can be closed applying moderate sphincter forces. Please note the closing of the hosepipe putting the hand around is unachievable. For sure, the hands allow closing the hosepipe through non-physiological actions such as twisting or bending, but one can easily imagine that such procedures would massively damage the rather fragile urethral tissue.

So far, the anatomy of the urethra has not attracted much attention, but since incontinence has been an essential problem in the aging society, artificial sphincters play a more and more important role. The commercially available implant systems, however, do not reach a satisfying level. Up to 50% of the AMS 800™ systems, for example, need revision during the first five years after implantation, although the implant system has been steadily improved during more than two decades [2-5]. Recently more sophisticated, nature-analogue artificial muscles are under development [6]. For their optimization the detailed microstructure of the tissue in open and closed states of the urethra has to be uncovered.

Micro computed tomography (μ CT) has been developed to a powerful technique for the characterization of hard and soft human tissues down to the sub-micrometer range. Because of its composition, hard tissues, in particular trabecular bone and teeth, can be perfectly evaluated by means of conventional micro computed tomography even in quantitative manner on true micrometer scale. Soft tissues including brain and urethra, however, are much more difficult to be analyzed, since the microstructures of interest exhibit very similar X-ray absorption than the surrounding tissues. Selective staining using highly absorbing species is an established approach, but here the tissue undergoes severe treatments. Similarly, embedding procedures can significantly improve the X-ray contrast [7-9], but lead to tissue modifications including shrinkage often related to the water exchange.

*bert.mueller@unibas.ch; phone +41 61 265 9660; fax +41 61 265 9699; www.bmc.unibas.ch

Therefore, the more recently developed phase contrast modes are especially accommodating in soft tissue tomography. The efforts for data acquisition and reconstruction, however, are much higher. The spatial resolution in grating-based phase contrast imaging is usually one order of magnitude worse than in absorption contrast mode. The quantitative interpretation of the 3D images is straightforward in absorption mode. One just obtains the local X-ray absorption. The phase retrieval in phase contrast modes, however, is demanding and sometimes even impossible. Hence many research teams just publish gray-level images without knowing the related quantities. Nevertheless, these images are certainly valuable especially if correlated with data of complementary techniques such as histology. In this context, grating interferometry [10], a fairly young method, is unique. Several examples of relatively large specimens show superior contrast at reasonable spatial resolution in the fully quantitative 3D datasets, for example [11].

The present contribution deals with the morphological characterization of urethral tissues from sheep, pig and human. So far, histology was the only technique applied to obtain the microstructure of the animal and human urethras. Three-dimensional studies, based on micro computed tomography, are unknown. Nevertheless, the micro-morphology of the urethra is of utmost importance to understand its function. As the number of incontinent patients is steadily increasing, the opening/closing the urethra under static and stress conditions has to be uncovered for the realization of artificial urinary sphincters. Although the engineers feel that the urethral sphincter can be described by a simple valve – usually closed and just opened to pass water, the actual situation is complex, as the tissue is fragile and has to work for decades.

The urethra compression model [12], for example, shows the complexity behind the closing mechanism. The model yields three empirical parameters for the tissue characterization, which allow differentiating between urethras of different animals. Due to similar size to humans, *in vivo* tests of artificial urinary sphincters are often performed in sheep. But extended *in vitro* studies analyzed by means of the urethra compression model demonstrated that the male human urethra resembles best the porcine one but show very different behavior with respect to sheep. The reasons behind are still not completely understood, because the microanatomy is only roughly investigated. Therefore, the present paper aims to elucidate anatomical similarities and differences between human, sheep and pig urethras to identify, which animal is the more appropriate one for *in vivo* testing of artificial urinary sphincters.

Synchrotron radiation-based micro computed tomography (SR μ CT) could support to discover the morphological similarities and differences between human and animal (pig, sheep) urethras on the micrometer scale. As the anatomy of the urethra drastically differs between males and females, the study includes both types of urethras.

2. MATERIALS AND METHODS

2.1 Sheep and porcine urethras

The animal specimens were approximately 10 mm-long parts of explanted urethras of domestic pig and sheep. They have been extracted from animals sacrificed for food production. Excess parts including bladder pieces were carefully removed, before the urethra has been cleaned using water.

One porcine specimen was fixed in a cylindrically shaped, water-filled container for grating-based SR μ CT in phase contrast mode.

The other specimens were embedded for SR μ CT in absorption contrast mode and histological analysis. First, the urethral tissues were fixated in a 5% formaldehyde solution. Second, the tissue was dehydrated in ascending alcohol series with concentrations of 50%, 70%, 80%, 90%, 96% and 100%. Each dehydration step took a time period of 24 h. Third, in order to remove the grease, the specimens were immersed in xylol for a period of five minutes. Finally, the tissue pieces were embedded in polymethylmetacrylate (PMMA). The embedding solution consisted of 40 ml methylmetacrylate, 10 ml dibutylphtalate (softener) and 1 g perkadox (activation agent). The polymerization took about 8 h at room temperature. Slices for optical microscopy were cut using a rotary microtome to return a thickness of 10 to 20 μ m.

For the histological analysis, the slices were colored with toluidin blue or according to giemsa staining. The images were recorded by means of the optical microscope (Leica).

2.2 Human urethras

One male and one female urethra were explanted post mortem at the Institute for Legal Medicine, University Hospital Hamburg-Eppendorf, Germany in accordance with the Declaration of Helsinki and according to the ethical guidelines of the University Hospital. The piece of interest, close to the bladder neck, was transferred into a phosphate buffer saline

filled container. This cylindrically shaped, polymer container was closed and immediately transported to the beamline W 2 (HASYLAB at DESY, Hamburg, Germany) for phase contrast imaging. The GKSS Research Centre operates the beamline including the tomography setup.

After the phase contrast imaging the urethras were fixated and embedded in PMMA as described above. Subsequently, the embedded specimens were made visible using SR μ CT in absorption contrast mode and prepared for the histological analysis as described for the animal urethras.

2.3 SR μ CT in absorption contrast mode

SR μ CT measurements in absorption contrast mode were performed at the beamline BW 2 (storage ring DORIS III, HASYLAB at DESY Hamburg, Germany), where the GKSS-Research Centre operates the μ CT-system as user experiment [13]. The experimental parameters are summarized in Table 1.

Table 1. Parameters for the tomography of embedded urethras in absorption contrast mode.

Specimen	Photon energy [keV]	Pixel size [μ m]	Spatial resolution [μ m]	# projections
Sheep, male	15	5.2	8.4	1440 (360°)
Pig, male and female	17	4.9	7.4	1440 (360°)
Human, male	18	4.2	6.6	2880 (360°)
Human, female	20	4.2	7.0	2880 (360°)

Using a highly X-ray absorbing edge, the spatial resolution of the experimental setup was determined by the 10% value of the modulation transfer function [14]. In order to increase the total field of view, the projections were acquired with an asymmetric rotation axis and 360° rotation, as described earlier [15]. For reconstruction by means of the filtered back projection algorithm two (or four) out of the 1440 (2880) projections were combined with pixel precision [15]. Therefore, 720 projections were used for the reconstruction by means of the filtered back-projection algorithm available for the beamline users. The data were binned by a factor of two to increase the density resolution [16]. As the urethra specimens were often exceeded the field of view, they were scanned at different height levels and combined to obtain one tomogram for each specimen. The related registration was done after the reconstruction with voxel precision.

2.4 Grating interferometry

The grating-based phase contrast measurements were performed at the beamline W 2 with the recently established grating interferometer setup [17]. The experimental parameters are summarized in Table 2.

Table 2. Parameters for the grating-based tomography of freshly explanted urethras in formalin solution and phosphate buffer saline, respectively.

Specimen	Photon energy [keV]	Pixel size [μ m]	Spatial resolution [μ m]	# projections
Pig, male	25	9.9	37	721 (180°)
Human, male	24	10.0	37	1101 (360°)
Human, female	24	10.0	37	501 (180°)

The spatial resolution of the experimental setup was determined by the 10% value of the modulation transfer function of a processed projection of a silicon wedge. The source grating g_0 had the periodicity of $p_0 = 22.3 \mu\text{m}$, the beam-splitter grating g_1 the periodicity of $p_1 = 4.33 \mu\text{m}$ and the analyzer grating g_2 the periodicity of $p_2 = 2.14 \mu\text{m}$. With a Talbot distance of 32.3 cm (6th Talbot order), the ratio of the grating periods, p_2/p_1 , was matched to the beam divergence. For the porcine urethra at each projection angle, eight phase-stepping images were taken over two periods of the interferometer fringe pattern, for the both human urethras six phase-stepping images over one period.

2.5 Data visualization

The software VGStudioMax 2.0 (Volume Graphics GmbH, Heidelberg, Germany) served for the visualization of the 3D data sets and the generation of slices perpendicular to each another.

3. RESULTS

3.1 Micro-morphology of sheep urethras

Although the urethra is composed of soft tissues, micro computed tomography in absorption contrast mode allows visualizing the characteristic layered morphology of the embedded sheep urethral tissue (see Figure 1). The brighter the tissue appears the higher is the X-ray absorption as quantitatively given by the gray scale bar that shows the X-ray absorption μ between 1.29 and 1.77 cm^{-1} . The opening/lumen of the urethra is surrounded by an epithelium, which forms together with the *lamina propria* the 1 to 2 mm-thick *tunica mucosa*. Caverns (appear black), as found in the *lamina propria*, are characteristic for connective tissue in mammals. As in histology, one can observe a clear interface between the *tunica mucosa* and the *tunica muscularis*, built of muscular tissue. Especially near this interface, the layered smooth muscles are perfectly reproduced in the tomography data.

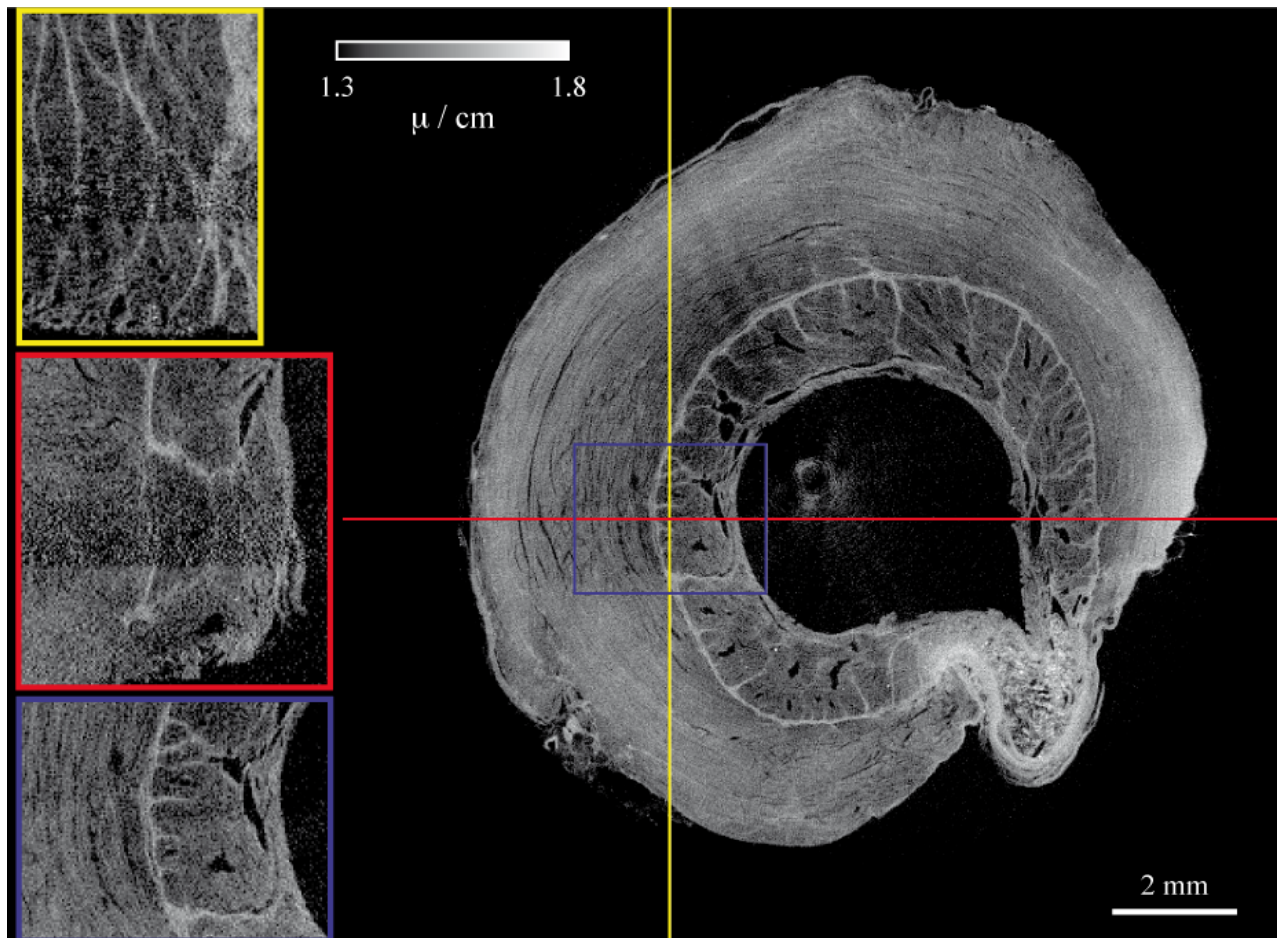


Figure 1. The selected slices represent the absorption contrast SR μ CT data of a PMMA-embedded sheep urethra (male), which were obtained at the beamline BW 2 using a photon energy of 15 keV.

3.2 Micro-morphology of porcine urethras in absorption contrast mode

Figure 2 shows SR μ CT data of embedded porcine urethras, which exhibit a variety of preparation and imaging artifacts, which make clear analysis as completed for the sheep urethra difficult. First, with the exception of the thick bloc one finds cracks often observed, when the embedding was done under some time pressure. Second, the slice top, left contains an artifact related to the imperfect overlay for the combination of projections from asymmetric rotation axis. Third, the contrast is much weaker than for the sheep urethra. A rough estimate leads to a reduction by a factor of 1.5. Forth, the stacking of the different height levels becomes visible by reduced photon statistics at the transition regions. Nevertheless, in the biggest bloc one can clearly identify the lumen surrounded by the epithelium. The layered structure of the *tunica muscularis* is seen best in the virtual slice parallel to the lumen on the right. An interface between the *tunica mucosa* and the *tunica muscularis*, as found for the sheep urethra, is not obvious, although the epithelium border to the lumen is clearly recognized.

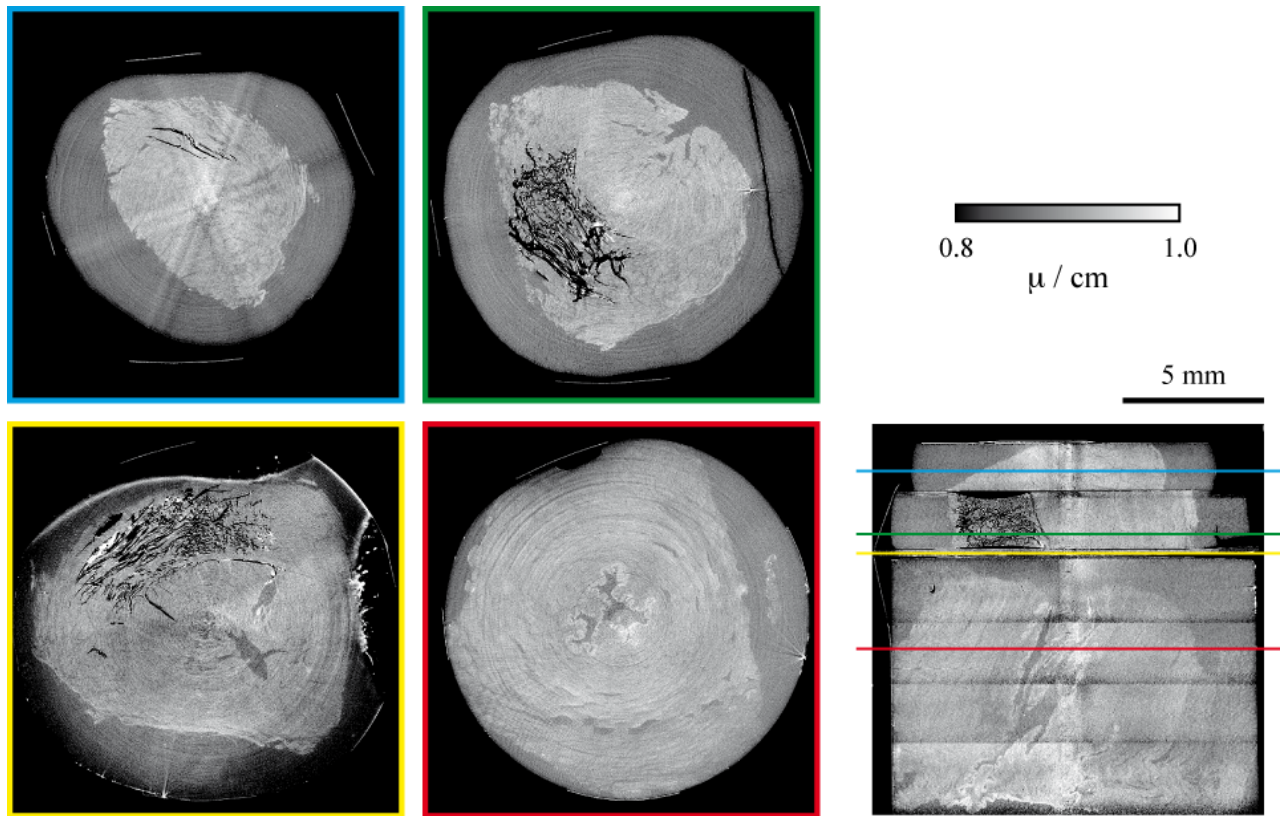


Figure 2. The images are virtual cuts through absorption contrast SR μ CT data of stacked PMMA-embedded porcine urethras obtained at the beamline BW 2 using a photon energy of 17 keV.

3.3 Micro-morphology of human urethras in absorption contrast mode

The human urethras visualized in Figure 3 exhibit similar preparation and imaging artifacts as the porcine tissue. For the male urethra in the top line of Figure 3, the lumen is clearly detected, which is verified from the optical micrograph of the section on the right. Note, the cracks appear in the micrograph as gray areas, whereas the lumen is transparent.

The selected SR μ CT slice is represented in different gray scales to show the indication of the *lamina propria* that exhibit slightly higher X-ray absorption than the *tunica muscularis*. Similar, the optical section also represents only vague signs of differentiations between *lamina propria* and *tunica muscularis*.

It should be noted that the contrast is even weaker for the human urethra than for the urethras of pig and sheep. Nevertheless, one recognizes the non-homogeneous smooth muscle, which also does not show the layered structure best seen in the sheep tissue.

The situation for the female urethra is even worse. The contrast is extremely weak and the preparation and imaging artifact so prominent that meaningful analysis becomes impossible. One can only state that the female urethra exhibits more homogeneous structures than the male urethral tissue.

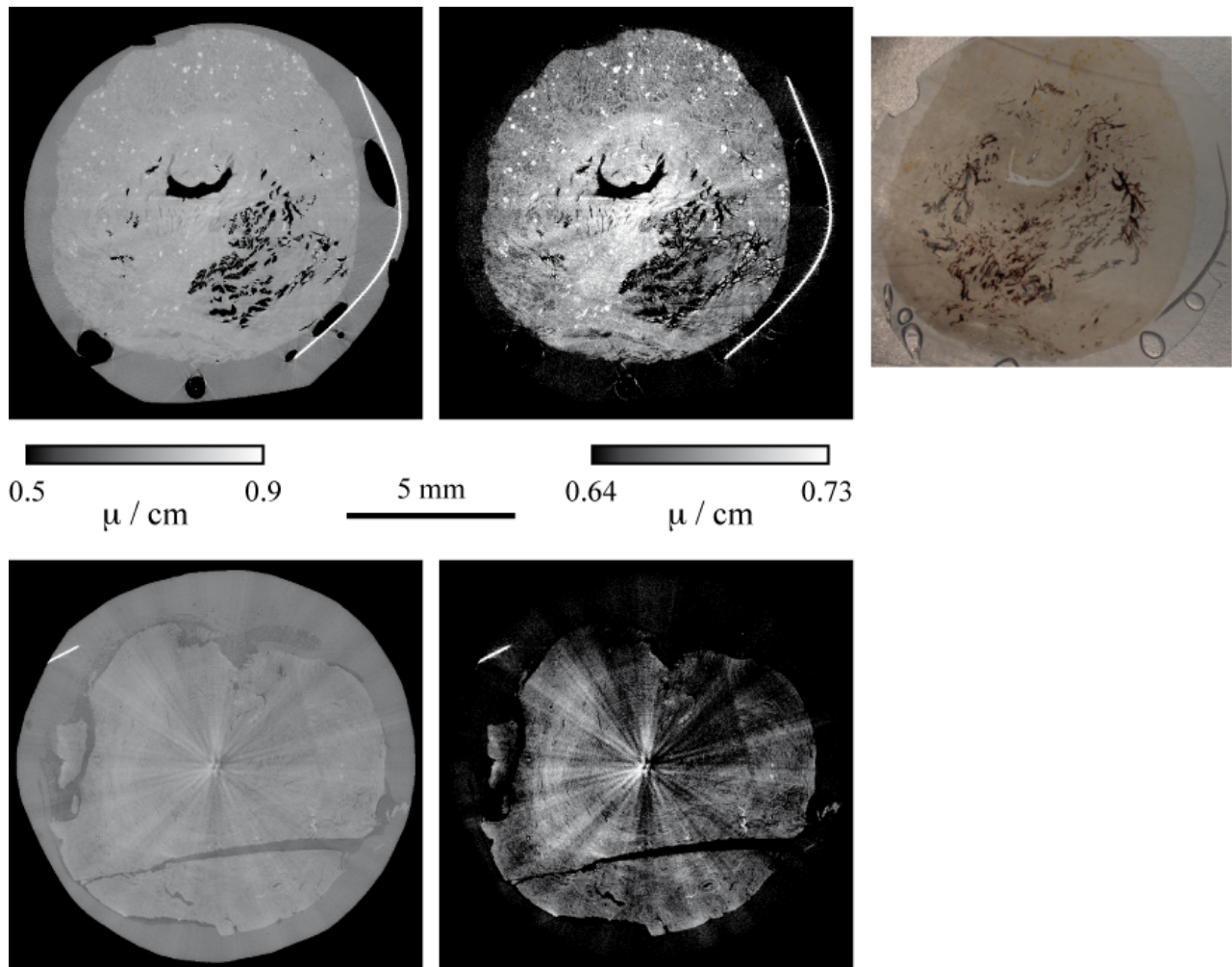


Figure 3. The selected virtual sections are derived from absorption contrast SR μ CT of PMMA-embedded male (top) and female (bottom) human urethras recorded at the beamline BW 2 with photon energies of 18 and 20 keV, respectively. The color image is a conventional optical section of the male urethra for comparison.

3.4 Micro-morphology of porcine urethras in phase contrast mode

The images of a porcine urethra obtained by phase contrast μ CT, see Figure 4, show the layered composition with much better contrast than the absorption contrast data. In agreement with previous histology results, the features are classified. The lumen with its irregular, branched shape is surrounded by the more or less homogeneous *tunica mucosa* that has a relatively high electron density. Around the *tunica mucosa* a ring-like structure appears related to the *tela submucosa*. The next layer visible is the *tunica muscularis*. This rather thick feature mainly consisting of muscle tissue induces inhomogeneous but rather small phase shifts. The different orientations of the muscle fibers may be responsible for the patterned structure. It could be also the result of cells arranged around the muscle fibers to be proven by the detailed analysis of the histological slices. These muscle fibers are known as axially orientated. The non-patterned area refers, hence, to the circularly orientated smooth muscles. Around the *tunica muscularis*, a third layer the *tunica adventitia* is clearly represented. The *tunica adventitia*, the outermost layer of the urethra, consists basically of low-dense connective tissue, which, however, exhibits also rather large phase shifts.

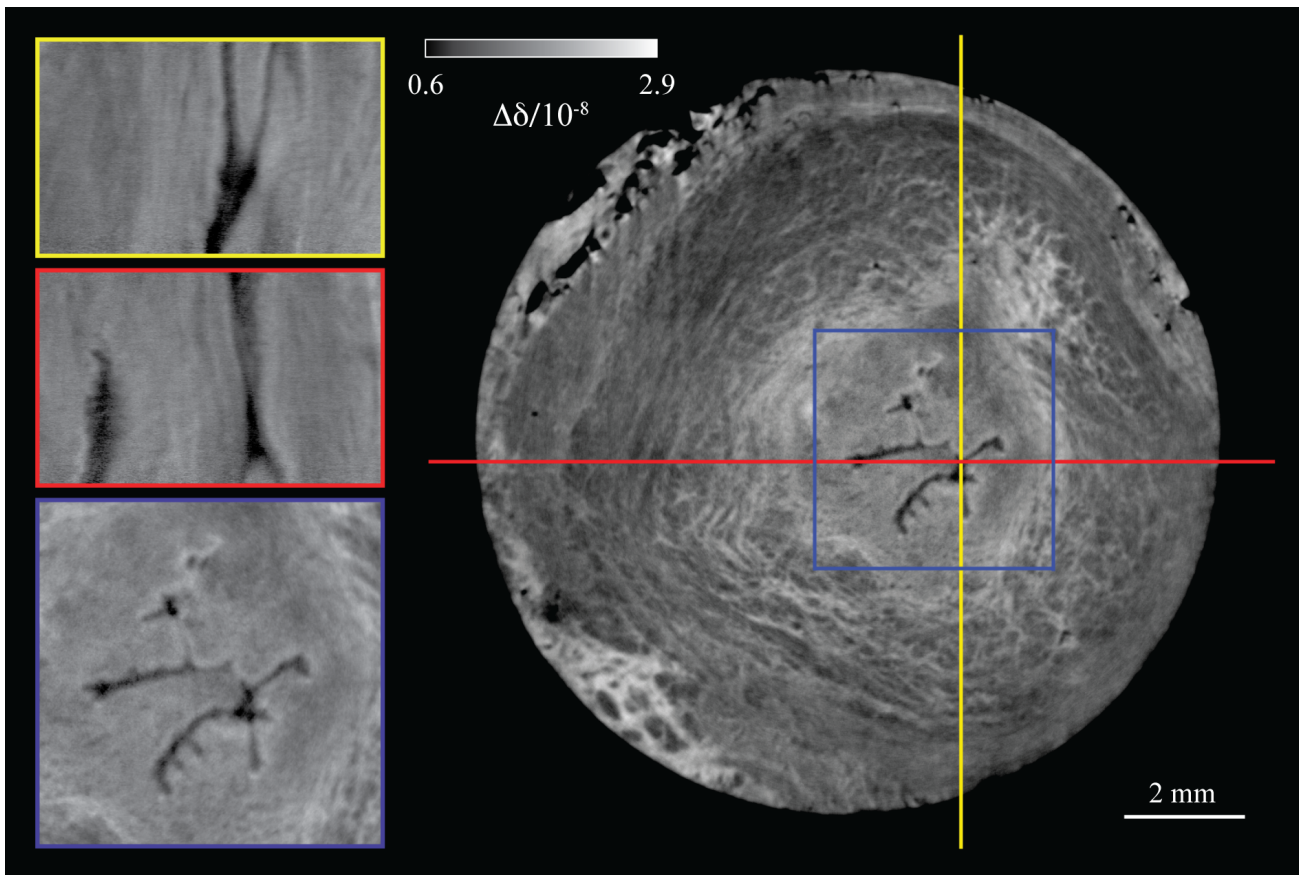


Figure 4. The images are virtual cuts of grating-based SR μ CT of a freshly explanted porcine urethra in phosphate buffer. The data were acquired at the GKSS-beamline W 2 (DORIS III, DESY, Hamburg, Germany) using a photon energy of 25 keV.

3.5 Micro-morphology of human urethras

Figure 5 represents the grating-based SR μ CT slices of the male human urethra. One finds many similarities between the images from the porcine urethra (see Figure 4) and the images of the human urethra. There are, however, some differences. First, the discrimination between the *tunica muscularis* and the *tunica mucosa* is very difficult, but manually possible. Second, the lumen of the partially closed urethra can be clearly identified in the images of Figure 5, but the epithelium is not visible.

The human male urethral tissue exhibits an anisotropic, layered structure in 3D with some symmetry along the lumen. This is quite similar to the porcine urethra. Nevertheless, one finds more pronounced anisotropic, layered structures in the *tunica mucosa*. Again, one recognizes patterned and non-patterned regions, which are more difficult to segment than in the case of the pig urethra.

Comparing the phase-contrast data in Figure 5 with the absorption-contrast tomography data in the top line of Figure 3 many similarities come to light including a brighter region around the lumen and an extended inhomogeneous patterned region around this brighter one. The patterned region, however, does not show the same morphology. Features such as the bright dots in the outer region of the urethra in the first line of Figure 3 are not found in the images of Figure 5.

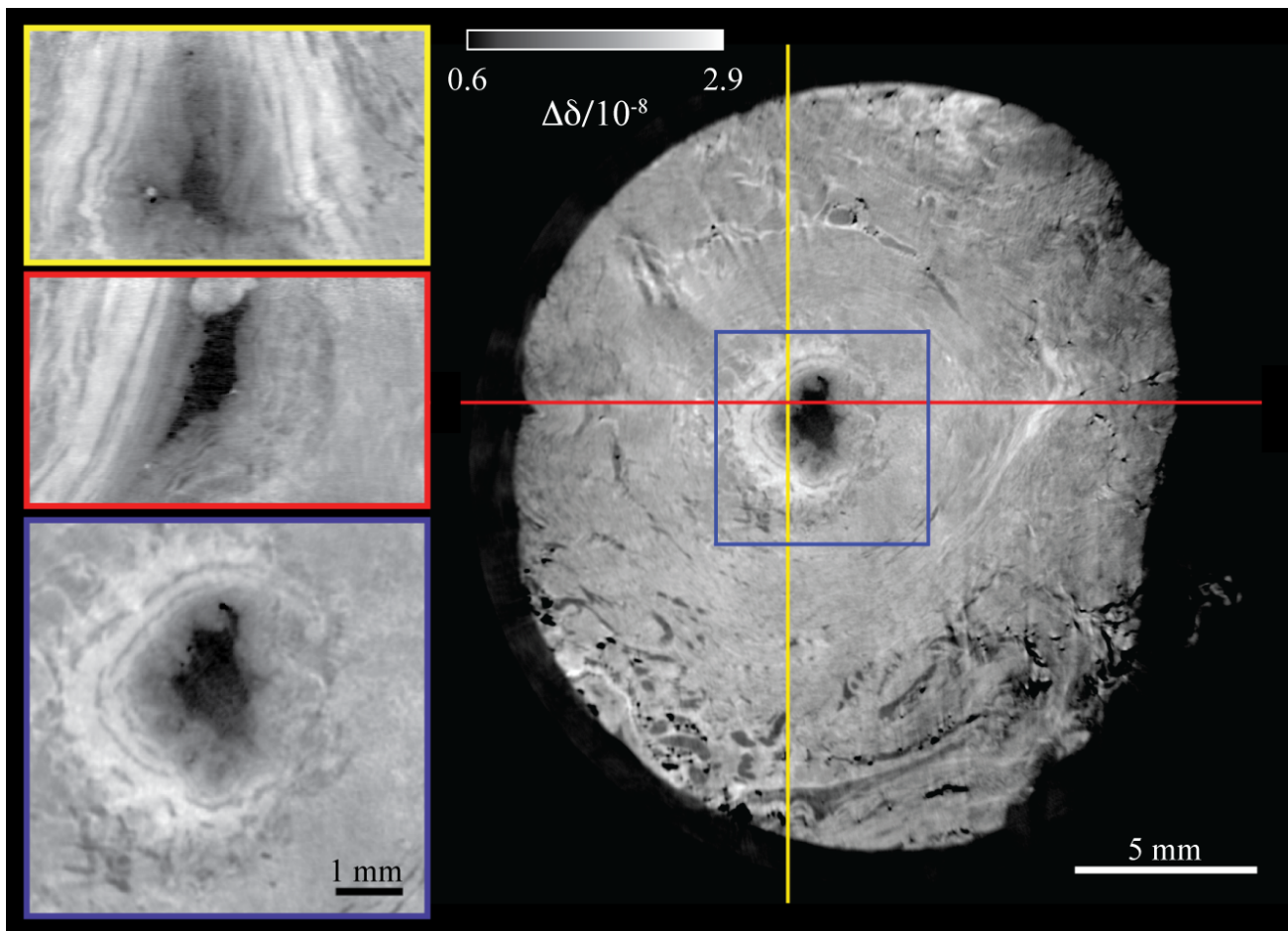


Figure 5. Grating-based SR μ CT data of a male human urethra measured at the GKSS-beamline W 2 with a photon energy of 24 keV: one recognizes from the three virtual cuts perpendicular to each other the non-perfect symmetry along the opening.

From the data represented in Figure 3, one can conclude that the male urethra is more inhomogeneous in structure than the female urethra. This is not surprising for urologists, since they experience this difference from everyday palpation. This general finding is also uncovered for the phase-contrast imaging performed.

The female urethra was somehow press-fit into the polymer container, so that the lumen is in closed state and not clearly seen in the image of Figure 6. Although the general features of the *tunica mucosa*, *tunica muscularis*, and *tunica adventia* show comparable contrast, the microanatomy between male and female urethra show significant differences, which can also explain the different mechanical behavior. For example, one recognizes well-separated features with $\Delta\delta$ of about $1.7 \cdot 10^{-8}$ for the male urethra but not for the female one. For the female urethra, a rather large part of urethral tissue at periphery shows a phase shift of the phosphate buffer. These features have sharp interfaces to the other soft tissue components.

The representative image of the female urethra exhibits imperfections. Most promising is the blurring in the upper part, which is really strong, so that the layered structure of the *tunica muscularis*, nicely reproduced in the lower part, is not seen any more. Since the blurring is due to the limited depth of focus for the present set-up of the detector, it can be avoided acquiring projections for 360° (as done for the data given in Figure 5) and not just for 180° specimen rotation at asymmetric rotation stage used for the present experiments.

The more liquid-like properties of the female urethra are also reflected in the reduced contrast with respect to the male tissue. The female tissue appears much more homogeneous easily understandable by the less muscular portion in the much shorter female urethra compared to the male one with different anatomical adjacent organs.

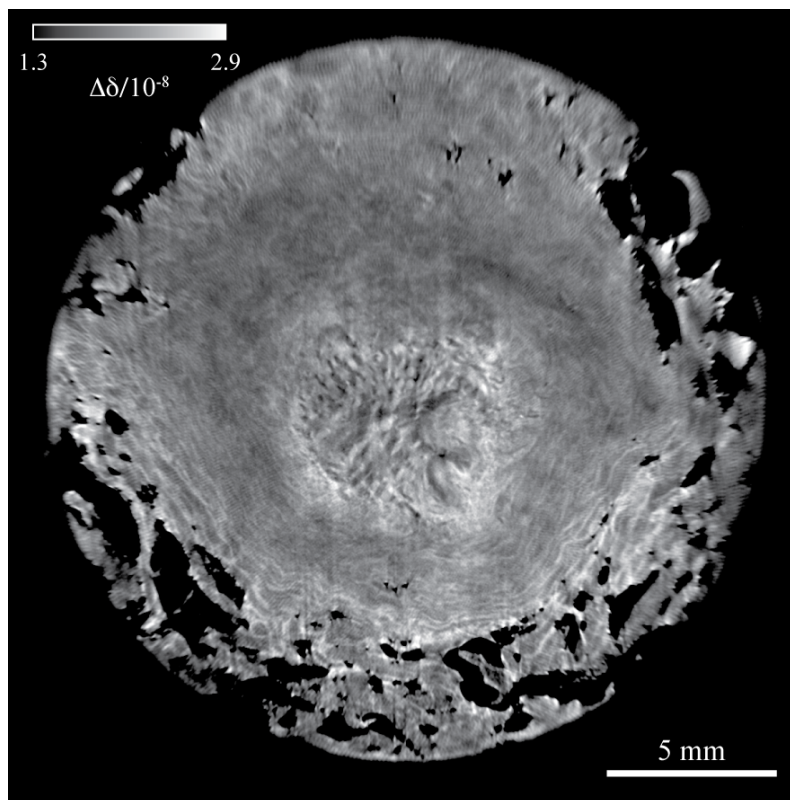


Figure 6. The grating-based SR μ CT data of a female urethra in closed state show the symmetry and the deviations from this symmetry as the result of the characteristic anatomy of females. The projections were recorded at the GKSS-beamline W 2 using a photon energy of 24 keV.

3.6 Determination of the contrast resolution

The contrast within tomography data can be characterized using the histograms of the entire 3D dataset [16]. The full width at half maximum (FWHM) of the individual peaks is given by the convolution of the instrumental broadening and the inhomogeneity of the related component within the specimen. Because of the inhomogeneity of the urethral tissues, we have chosen the water peak for characterizing the resolution in refractive index of the phase-contrast experiments.

Figure 7 contains the histograms of grating-based tomography data of porcine urethra (left part, data as visualized in Figure 4) and male human urethra (right part, data as given in Figure 5). The peak related to the water surrounding the specimen container is very close to $\Delta\delta = 0$ and fitted by means of a single Gaussian. For the entire 3D dataset (bulk), the FWHM corresponds to $(5.85 \pm 0.04) \cdot 10^{-10}$ in case of pig and to $(5.55 \pm 0.07) \cdot 10^{-10}$ in case of the human urethra. Note, these values of the FWHM are only slightly larger or even identical to the ones of a typical slice, which indicates no significant change from slice to slice.

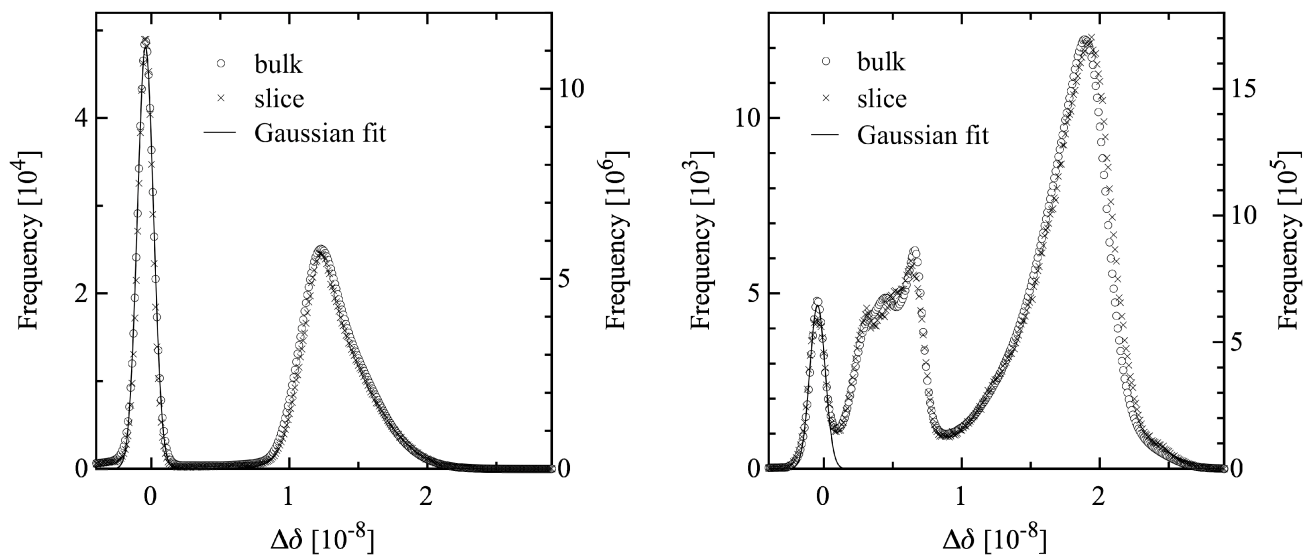


Figure 7. Histograms of tomography data from porcine (left) and human (right) urethras: There is no significant difference between selected 2D data (slice) and the entire 3D dataset (bulk), which are scaled according to the right and left Y-axes, respectively.

4. DISCUSSION

The present study demonstrates that SR μ CT in absorption and phase contrast modes allows visualizing animal and human urethras to elucidate their rather complex inhomogeneous and anisotropic anatomy on the micrometer scale. There are substantial differences between the sheep and human urethras as previously verified by means of the urethra compression model and related in vitro experiments [18]. The microanatomy of the porcine urethra resembles much better the male human ones, which correlates to the similarities in the mechanical properties. The stiffness of urethral tissues is highest for sheep, significantly lower but still relatively high for boar, further lower for sow – but comparable to human male and even lower for human female urethral tissue. Therefore, one may conclude that the mechanical properties are in-line with the microanatomy and the contrast differences from features in SR μ CT.

The features uncovered using SR μ CT have to be related to conventional histology results to discover how far SR μ CT can yield additional information. This analysis needs some effort especially since the phase-contrast data have to be non-rigidly registered with the histological images.

The grating-based interferometry experiments belong to the first successful measurements performed at the GKSS-beamline W 2 [17]. The resolution power of this setup can be deduced from the real part of the refractive index $\Delta\delta$ and is

only a factor of four worse than the advanced ID 19 experiment at ESRF, France [19] and within a factor of two for an ID 19 measurement of a soft tissue sample with comparable geometry [11]. The peak broadening for the ID 19 data, which originates from slight $\Delta\delta$ shifts along the rotation axis, is not observed at the present setup indicating a reasonable stability of the data acquisition. Further improvements, however, are necessary to reach the level of the best instruments worldwide.

5. CONCLUSION

The present communication on the microanatomy of animal and human urethras shows that porcine urethras resemble best the human ones. Therefore, animal studies to test artificial urinary sphincters should be performed by means of pigs and not by means of sheep as often performed today.

The experimental setup for grating-based phase-contrast tomography at the beamline W 2 (DORIS III at DESY, Hamburg, Germany) operated by the GKSS Research Centre (second-generation synchrotron radiation source) permits the acquisition of data that are comparable to data recorded at the highly advanced third-generation synchrotron radiation sources. This instrument will become a user-experiment soon and the community is invited to submit scientific proposals for beamtime.

REFERENCES

- [1] Griffiths, D., "The pressure within a collapsed tube, with special reference to urethral pressure," *Phys. Med. Biol.* 30(9), 951-963 (1985).
- [2] Hajivassiliou, C. A. and I. G. Finlay, "Uneven pressure application by the artificial urinary sphincter: an explanation for tissue ischaemia?," *Brit. J. Urol. Int.* 83(4), 416-419 (1999).
- [3] Hussain, M., T. J. Greenwell, S. N. Venn et al., "The current role of the artificial urinary sphincter for the treatment of urinary incontinence.," *J. Urol.* 174(2), 418-424 (2005).
- [4] Maillot, F., J. M. Buzelin, O. Bouchot et al., "Management of artificial urinary sphincter dysfunction.," *Eur. Urol.* 46(2), 241-245 (2004).
- [5] Mourtzinou, A., J. J. Smith, and D. M. Barrett, "Treatments for male urinary incontinence: A review," *AUA Update Series* 24, 121-132 (2005).
- [6] Müller, B., H. Deyhle, S. Mushkolaj et al., "The challenges in artificial muscle research to treat incontinence," *Swiss Medical Weekly* 139(41-42), 591-595 (2009).
- [7] Müller, B., J. Fischer, U. Dietz et al., "Blood vessel staining in the myocardium for 3D visualization down to the smallest capillaries," *Nucl. Instrum. Meth. B* 246, 254-261 (2006).
- [8] Müller, B., M. Germann, D. Jeanmonod et al., "Three-dimensional assessment of brain tissue morphology," *Proc. SPIE* 6318, 631803 (2006).
- [9] Plouraboue, F., P. Cloetens, C. Fonta et al., "X-ray high-resolution vascular network imaging," *J. Microsc.* 215(2), 139-148 (2004).
- [10] Weitkamp, T., A. Diaz, C. David et al., "X-ray phase imaging with a grating interferometer," *Optics Express*, 13(16), 6296-6304 (2005).
- [11] Schulz, G., T. Weitkamp, I. Zanette et al., "High-resolution tomographic imaging of a human cerebellum: comparison of absorption and grating-based phase contrast," *J. Royal Soc. Interface* (2010).
- [12] Marti, F., T. Leippold, H. John et al., "Optimization of the artificial urinary sphincter: modelling and experimental validation," *Phys. Med. Biol.* 51(5), 1361-1375 (2006).
- [13] Beckmann, F., J. Herzen, A. Haibel et al., "High density resolution in synchrotron-radiation-based attenuation-contrast microtomography," *Proc. SPIE* 7078, 70781D (2008).
- [14] Müller, B., P. Thurner, F. Beckmann et al., "Non-destructive three-dimensional evaluation of biocompatible materials by microtomography using synchrotron radiation," *Proc. SPIE* 4503, 178-188 (2002).
- [15] Müller, B., R. Bernhardt, T. Weitkamp et al., "Morphology of bony tissues and implants uncovered by high-resolution tomographic imaging," *Int. J. Mater. Res.* 98(7), 613-621 (2007).

- [16] Thurner, P., F. Beckmann, and B. Müller, "An optimization procedure for spatial and density resolution in hard X-ray micro-computed tomography," *Nucl. Instrum. Meth.* 225(4), 599-603 (2004).
- [17] Herzen, J., F. Beckmann, T. Donath et al., "X-ray grating interferometer for imaging at a second-generation synchrotron radiation source," *Proc. SPIE* 7804, (2010).
- [18] Marti, F., T. Leippold, H. John et al., "Optimization of the artificial urinary sphincter: modelling and experimental validation," *Phys. Med. Biol.* 51(5), 1361-1375 (2006).
- [19] Pfeiffer, F., C. David, O. Bunk et al., "High-sensitivity phase-contrast tomography of rat brain in phosphate buffered saline," *J. Phys.: Conference Series* 186, 012046 (2009).